1080 *Chem. Mater.* **2010,** *22,* 1080–1087
DOI:10.1021/cm9020782

CHEMISTRY OF MATERIALS
Article

Improved Fuel Cell Oxidation Catalysis in $Pt_{1-x}Ta_x$[†]

John M. Gregoire,[‡] Michele E. Tague,[§] Sophie Cahen,[⊥] Sahr Khan,[∥] Héctor D. Abruña,[§] Francis J. DiSalvo,[§] and R. Bruce van Dover*[,#]

[‡]*Department of Physics and* [§]*Department of Chemistry and Chemical Biology and* [#]*Department of Material Science and Engineering, Cornell University, Ithaca, New York 14853,* [⊥]*Ecole Centrale Paris, Paris, France, and* [∥]*Wellesley College, Wellesley, Massachusetts 02418*

Received July 9, 2009. Revised Manuscript Received October 18, 2009

Sputter codeposition of platinum and tantalum is used to generate catalyst libraries of $Pt_{1-x}Ta_x$ with $0.05 < x < 0.9$. Extensive characterization of the libraries by high-energy X-ray diffraction reveals the presence of several ordered intermetallic phases as a function of composition and deposition conditions. Assessment of the activity toward the oxidation of methanol and formic acid is achieved through a fluorescence-based parallel screening, followed by detailed testing of the most promising catalysts. Correlations among the electrochemical results, the inferred phase fields and X-ray photoelectron spectroscopy characterization provide an understanding of the catalytically active surface and highlight the utility of composition spread thin films in catalyst research. The observations suggest that the interaction between Pt and Ta suboxides is important and enhances the catalytic activity of Pt.

Introduction

Fuel cells, in particular polymer electrolyte membrane fuel cells (PEMFCs), represent an attractive technology to meet future energy needs because of their potentially high efficiency in converting stored chemical energy to electrical energy. However, their widespread deployment has been hampered by materials limitations, as exemplified in the catalysts by their high cost, intolerance to fuel contaminants, and degradation leading to short fuel cell lifetimes. The possible use of methanol and other small organic molecules (SOMs) as PEMFC fuels is promising because of their high energy density and ease of transport, compared to H_2. Presently, one of the setbacks for implementation of SOM PEMFCs has been the lack of an anode catalyst that effectively overcomes the kinetic barriers for complete oxidation (to CO_2) of these complex molecules. Theoretical models that describe the complete oxidation of SOMs incorporate several adsorption and charge transfer steps that are optimized by surface atomic and electronic structure properties unique to the catalyst.[1,2] During this oxidation process, CO formation (as an intermediate) is likely, and thus CO tolerance of catalysts is an implicit factor in oxidation catalysis studies using such fuels. CO tolerance is a particularly relevant property, as it is also of importance for the anode catalyst in H_2 fuel cells. The poisoning of Pt catalysts by CO impurities associated with H_2 production from hydrocarbon reformation is a quintessential issue in catalysis. To address this and other issues, catalyst research often involves the generation of a new catalyst by alloying Pt with less-noble metals (including Pt-based ordered intermetallics),[3] forming layered catalyst structures,[4,5] or replacing the standard carbon support for Pt nanoparticles. Because the interfaces among electrode components often play an important role in catalysis and the electrode surface may be altered during operation as a catalyst, these ideal electrode archetypes are rarely distinctly realized. The influence of electrode modification on catalytic activity is most directly determined by characterization of the surface during catalysis, a notoriously difficult task. In the present work, we present an ensemble of characterizations that, when applied to a library of catalysts in the Pt−Ta system, provide insights into the composition and structure of the most catalytically active material.

Tantalum Incorporation in Fuel Cell Catalysts. Recently, several methods of Ta inclusion in PEMFC electrode materials have been investigated. Ishihara et al.[6] demonstrated activity of partially oxidized tantalum carbonitrides for the oxygen reduction reaction (ORR) and noted the importance of the degree of surface oxidation. ORR catalysis was also studied on electrodes containing a combination of Vulcan carbon, Pt colloids and

[†] Accepted as part of the 2010 "Materials Chemistry of Energy Conversion Special Issue".

*Corresponding author. E-mail: vandover@cornell.edu.

(1) Frelink, T.; Visscher, W.; van Veen, J. A. R. *Surf. Sci.* **1995**, *335*, 353.
(2) Leger, J. M. *J. Appl. Electrochem.* **2001**, *31*, 767.
(3) Casado-Rivera, E.; Volpe, D.; Alden, L.; Lind, C.; Downie, C.; Vazquez-Alvarez, T.; Angelo, A.; DiSalvo, F.; Abruna, H. *J. Am. Chem. Soc.* **2004**, *126*, 4043.
(4) Lee, H.; Habas, S. E.; Somorjai, G.; Yang, P. *J. Am. Chem. Soc.* **2008**, *130*, 5406.
(5) Spendelow, J.; Lu, G.; Kenis, P.; Wieckowski, A. *J. Electroanal. Chem.* **2004**, *568*, 215.
(6) Ishihara, A.; Doi, S.; Mitsushima, S.; Ota, K. *Electrochim. Acta* **2008**, *53*, 5442.

 Published on Web 11/02/2009

TaO_y formed by oxidation of Ta after its reduction from $TaCl_5$. The addition of Ta_2O_5 increased the area-specific ORR activity for only certain $Pt-Ta_2O_5-C$ configurations, suggesting that any improvement in catalytic activity is related to the interfaces of the three components. $Pt_{1-x}Ta_x$ alloys have also been investigated as possible PEMFC cathode materials.[7] Composition spread thin films covering the entire composition range were found to be quite stable at oxidizing potentials in acidic media, but the catalytic activity for oxygen reduction dropped sharply and monotonically with increasing Ta content.

Studies of H_2 and CO oxidation have also been performed on TaO_y-modified Pt/C electrodes. CO oxidation on commercial Pt/C electrodes partially coated with Ta_2O_5 showed a 150 mV negative shift in the peak potential for oxidation of adsorbed CO.[8] Similar experiments were performed on $Pt + TaO_y$ and $PtRu + TaO_y$ electrodes.[9] The former electrode was made by coreduction of $Pt(NO_2)_2(NH_3)_2$ and $TaCl_5$ on Vulcan carbon. While the inclusion of TaO_y only lowered the CO oxidation peak by 70 mV (50 mV for $PtRu + TaO_y$), the authors also studied the time dependence of CO adsorption onto the electrodes and found that the inclusion of TaO_y significantly decreased the adsorption rate. This behavior indicates that the role of TaO_y in improving the CO tolerance of Pt is distinct from that of alloyed Ru. Surface Ru serves as a source of active oxygen and thus enhances CO oxidation,[10] but TaO_y diminishes the adsorption of CO, possibly through a decrease in the Pt-CO bond strength. The Ta oxidation state was not characterized in the materials of Ueda et al.,[9] but Lesnyak et al.[11] found that the use of a similar material as a gas phase H_2 oxidation catalyst resulted in partial reduction of the Ta_2O_5 support. The electrode, consisting of Pt nanoparticles on a Ta_2O_5 support, was characterized by XRD, electron diffraction and X-ray spectral microanalysis both before and after use as a catalyst for oxidation of H_2 in a fuel stream with 20:1 O_2:H_2. The catalysis test resulted in a decrease in the oxygen stoichiometry from $y = 2.4$ to 2.3, with both values slightly smaller for TaO_y regions adjacent to Pt particles. This partial reduction of the Ta caused the surface of the highly crystalline Ta_2O_5 support to transform into a nanocrystalline $Ta_2O_5 + TaO_2$ composite.

CO oxidation on $Pt_{1-x}Ta_x$ alloy thin films[12] and bulk Pt_2Ta and Pt_3Ta ordered intermetallics[13] has also been studied. The latter work found that the oxidation of adsorbed CO was shifted to more positive potentials for the intermetallic compounds compared to pure Pt. This shift could be due to an increase in Pt−CO binding energy and underscores a difference in the role of Ta in these materials and that of the $Pt-TaO_y$ composites. Stevens et al.[12] studied thin film $Pt_{1-x}Ta_x$ catalysts deposited on water-cooled substrates, and XRD characterization of the films indicated that the low deposition temperature kinetically stabilized Ta-rich bcc and Pt-rich fcc alloys. In addition, a nanocrystalline (or possibly amorphous) alloy (NCA) was observed for $x > 0.3$. The thin film samples with $0.3 < x < 0.7$ exhibited CO stripping onset potentials up to 50 mV lower than that of pure Pt and a corresponding small decrease in onset potential was observed for the oxidation of H_2 in the presence of CO.

We studied $Pt_{1-x}Ta_x$ composition spread thin films deposited at elevated temperatures, which enables the synthesis and electrochemical characterization of the ordered intermetallic phases. These films do contain an NCA region, and methanol oxidation on the as-deposited NCA demonstrates a negative shift in oxidation potential (in agreement with Stevens et al.).[12] However, we demonstrate further improvement in methanol oxidation activity via a catalyst pretreatment step. In addition, our study of methanol oxidation as a continuous function of composition, combined with the XRD mapping of the libraries, reveals important trends in catalytic activity.

Experimental Section

Composition Spread Deposition. Films were prepared in a custom built combinatorial sputter deposition system described previously.[14] Each $Pt_{1-x}Ta_x$ library was generated by first depositing an adhesion layer (underlayer) onto a 76.2 mm diameter Si substrate. During and after this deposition, the substrate was radiatively heated and maintained at the library deposition temperature. Elemental Pt and Ta (>99.9% purity) were codeposited from separate magnetron sputter sources (Angstrom Sciences) in an atmosphere of 0.66 Pa Ar. With the aid of a cryoshroud,[14] the background pressure during deposition remained in the 10^{-5} Pa range. The geometrical relation of the deposition sources with respect to the Si substrate provided a deposition gradient from each source that upon codeposition resulted in a continuous variation in composition across the substrate. The Pt and Ta deposition rates at substrate center were measured with a quartz crystal monitor just prior to deposition of the library.

The range of x represented in a given library is dictated by the deposition profiles of the individual sources but may be shifted to the Pt-rich or Ta-rich range by control of the relative power delivered to the independent sources. Given the constant deposition rates, the film thickness is determined by deposition time, but the thickness at each substrate position is determined by the local deposition rates and chemical mixing of the elements. In the present work, three $Pt_{1-x}Ta_x$ libraries are discussed; they are distinguished by the underlayer, deposition temperature, thickness at substrate center ("library thickness") and stoichiometry at substrate center. Library A was generated with a 12 nm Ti underlayer, 400 °C deposition

(7) Bonakdarpour, A.; Löbel, R.; Sheng, S.; Monchesky, T. L.; Dahn, J. R. *J. Electrochem. Soc.* **2006**, *153*, A2304.
(8) Yamada, Y.; Ueda, A.; Shioyama, H.; Kobayashi, T. *Appl. Surf. Sci.* **2004**, *223*, 220.
(9) Ueda, A.; Yamada, Y.; Ioroi, T.; Fujiwara, N.; Yasuda, K.; Miyazaki, Y.; Kobayashi, T. *Catal. Today* **2003**, *84*, 223.
(10) Watanabe, M.; Motoo, S. J. *Electroanal. Chem. Interfacial Electrochem.* **1975**, *60*, 275.
(11) Lesnyak, V. V.; Yatsimirskii, V. K.; Boldyreva, O. Y.; Kinder, T. D. *Theor. Exp. Chem.* **2008**, *44*, 189.
(12) Stevens, D. A.; Rouleau, J. M.; Mar, R. E.; Bonakdarpour, A.; Atanasoski, R. T.; Schmoeckel, A. K.; Debe, M. K.; Dahn, J. R. *J. Electrochem. Soc.* **2007**, *154*, B566.
(13) de los Santos-Alvarez, N.; Alden, L.; Rus, E.; Wang, H.; DiSalvo, F.; Abruna, H. *J. Electrochem. Soc.* **2009**, *626*, 14.
(14) Gregoire, J. M.; van Dover, R. B.; Jin, J.; DiSalvo, F. J.; Abruña, H. D. *Rev. Sci. Instrum.* **2007**, *78*, 072212.

temperature, 160 nm library thickness and $x = 0.25$ at substrate center. Library B was generated with a 12 nm Ta underlayer, 550 °C deposition temperature, 160 nm library thickness, and $x = 0.5$ at substrate center. Library C was generated with a 30 nm Ti underlayer, 450 °C deposition temperature, 35 nm library thickness, and $x = 0.33$ at substrate center.

Thin Film Characterization. We calculated the spatial map of composition in the libraries using verified models and measured deposition profiles for the Pt and Ta sources.[15,16] For Library A, composition measurements were made before electrochemical testing by X-ray fluorescence (XRF) with a 60 keV X-ray source[17] and after electrochemical testing by energy-dispersive X-ray spectroscopy (EDS) using a JEOL 8900 EPMA Microprobe. The composition maps from the three measurement techniques agree within the measurement errors. In this manuscript, the deposition profile-calculated compositions are used for all three libraries, and the additional data for Library A are presented in the Supporting Information.

XRD characterization of the libraries was performed with a high-throughput crystallography setup, which will be described in detail in a separate publication.[17] Monochromatic 60 keV X-rays impinge the thin film and the diffraction image is attained in transmission geometry by a 345 mm diameter image plate (Mar Research). Integration of the images provides diffraction patterns which are compared to patterns of known phases in the Powder Diffraction File (PDF)[18] to construct a phase map of the library. We also note that sputter deposition commonly yields fiber textured thin films in which the constituent crystallites are randomly oriented with respect to substrate azimuth but aligned with respect to substrate normal.[19] The average crystallite orientation in the film is determined by analyzing the diffraction images, as described in the Supporting Information. This orientation is important, as it dictates the crystal facet at the film surface, which may ultimately determinesurface chemistry and reactivity.

Surface composition and oxidation were characterized by XPS analysis using a Surface Science Instruments SSX-100 with a 1 μPa base pressure. Sample orientation provided a 55°emission angle. Survey scans were performed with 150 V pass energy from 0 to 600 eV at 1 eV/step. High resolution scans were performed with 50 V pass energy from 15 eV to 85 eV at 0.065 eV/step. In situ cleaning of the film surface was performed by 15 s impingement of 4 keV Ar at 3 μA/cm^2, but minor residual surface contamination by hydrocarbons was inferred from the presence of a weak C 1s peak. Although such contamination has a negligible effect on the analysis of the Ta and Pt, the likely presence of oxygen in the contaminant layer confounds the measurement of oxygen in the film.

The 15−85 eV spectra were fit with one set of Pt 4f doublet peaks and either two or three sets of Ta 4f doublet peaks using the CasaXPS software package. Our established analysis of metal thin films employs the Shirley line shape to model the background and an asymmetric-Lorentzian peak shape. For fitting procedures, the doublet peaks were constrained by the known binding energy shifts and area ratios.

Fluorescence Assay. In the past decade, a number of publications have presented combinatorial high-throughput methods for efficient exploration of the wide range of possible anode catalysts for direct methanol fuel cells (DMFCs). The fluorescence assay used to screen catalysts was first employed by Reddington[20] and further adapted for thin films by Prochaska, et al.[21] The entire film is used as the working electrode in a specially designed electrochemical cell.[22] In the screening process, a pH-sensitive fluorescent indicator is used to identify catalytically active regions in a combinatorial library.[21] The potential applied to the film is swept from −100 to 500 mV vs Ag/AgCl at a scan rate of 5 mV/s, and a large area Au coil serves as the counter electrode. The testing solution consists of 5 M methanol, 3 mM quinine, and 0.1 M potassium triflate as supporting electrolyte. The solution begins at neutral pH and as increasingly high overpotentials are applied to the film and methanol is oxidized, the released protons cause a decrease in pH below 5. Protonation of the quinine ensues and in this condition the quinine is fluorescent under UV illumination. Although the entire library is a common working electrode, the local generation of protons allows measurement of catalytic activity with $\lesssim$1 mm resolution via optical detection of fluorescence. Images are taken at 20 mV intervals with a charge-coupled device (CCD) camera, and at a given region of the library, image processing provides a fluorescence intensity voltammogram.

We previously presented[22] a model of this fluorescence profile of a Nernstian oxidation reaction

$$F = An\ln(1 + \mathrm{Exp}((E - E_{1/2})n/f)) \quad (1)$$

where F is the fluorescence intensity, E is the applied potential, and $f = 59.1$ mV at ambient temperature. The prefactor A, half-wave potential $E_{1/2}$, and number of electrons n in the rate-limiting reaction are model parameters. In the present work, we fix $n = 2$ and extract the figure of merit $E_{1/2}$ through least-squares fitting of the measured profiles.

In addition to the routine fluorescence tests, a pretreatment of the film is performed to ostensibly reduce surface oxides that are formed upon air exposure and to remove other surface contaminants. This pretreatment entails a linear voltage sweep from 0 to −800 mV vs Ag/AgCl in an aqueous solution of 0.01 M H_2SO_4 with 1 M Na_2SO_4 as supporting electrolyte.[22]

Localized Electrochemical Characterization. While the fluorescence assay allows us to efficiently identify the nominal compositions of promising methanol catalysts, additional testing is required to determine the catalytic properties under fuel cell (low pH) conditions. Localized electrochemical testing is enabled with a 6 mm inner diameter Teflon cell that isolates a 0.32 cm^2 film region. A 70 mm diameter cell seals on the edge of the substrate and is filled to expose the entire library (working electrode) to testing solution. The 6 mm cell contains counter and reference electrodes, and positioning the cell at a chosen spot on the substrate allows for testing of catalysts within a 5 at % composition range. In the present study, this technique is used to acquire cyclic voltammograms (CVs) of select catalyst

(15) Gregoire, J. M.; Lobovsky, M. B.; Heinz, M. F.; DiSalvo, F. J.; van Dover, R. B. *Phys. Rev. B* **2007**, *76*, 195437.
(16) Gregoire, J. M.; van Dover, R. B. *J. Vac. Sci. Technol., A* **2008**, *26*, 1030.
(17) Gregoire, J. M.; Dale, D.; Kazimirov, A.; DiSalvo, F. J.; van Dover, R. B. Private communication, **2009**.
(18) *Powder Diffraction File*; JCPDS International Centre for Diffraction Data: Newtown Square, PA 2004.
(19) Ohring, M. *Materials Science of Thin Films*, 2nd ed.; Academic Press: New York, 2002.
(20) Reddington, E.; Sapienza, A.; Gurau, B.; Viswanathan, R.; Sarangapani, S.; Smotkin, E. S.; Mallouk, T. E. *Science* **1998**, *280*, 1735.
(21) Prochaska, M.; Jin, J.; Rochefort, D.; Zhuang, L.; DiSalvo, F. J.; Abruna, H. D.; van Dover, R. B. *Rev. Sci. Instrum.* **2006**, *77*, 154104.
(22) Gregoire, J. M.; Kostylev, M.; Tague, M. E.; Mutolo, P. F.; van Dover, R. B.; DiSalvo, F. J.; Abruna, H. D. *J. Electrochem. Soc.* **2009**, *156*, B160.

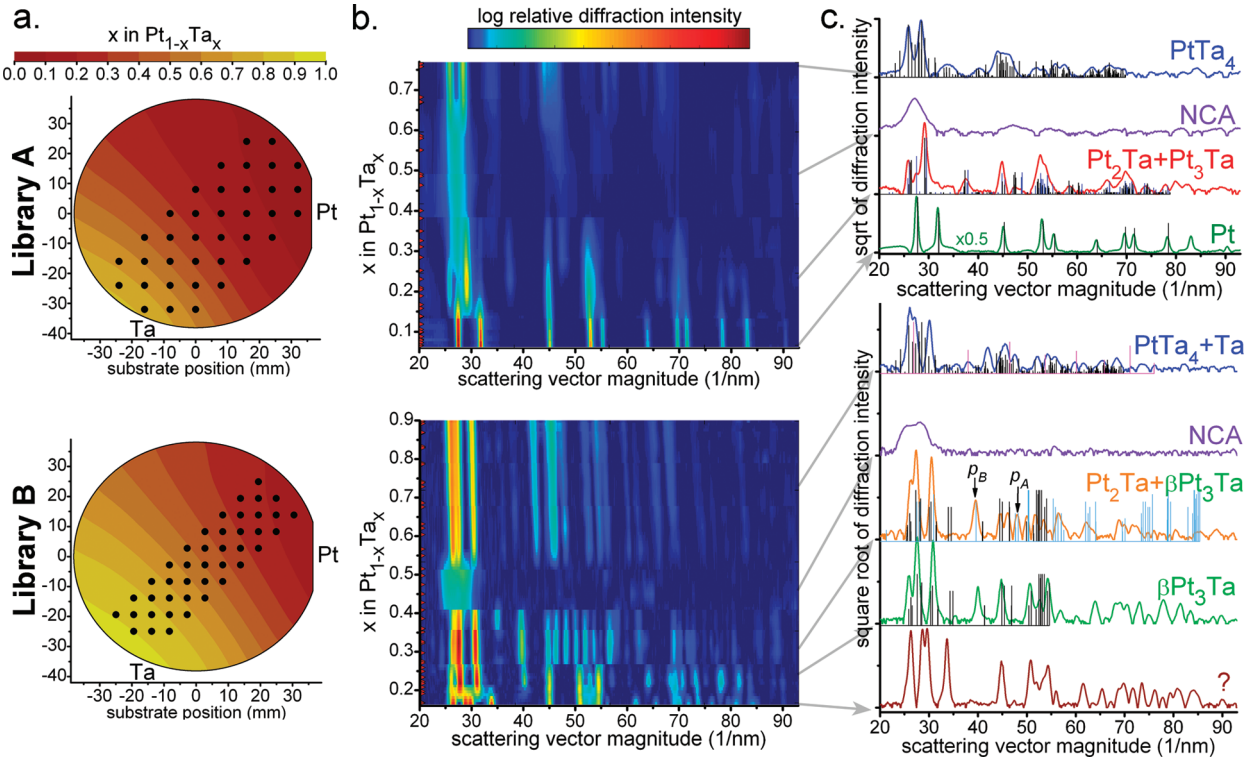

Figure 1. Composition and XRD mapping of Libraries A (top row) and B (bottom row). (a) Value of Ta fraction x as calculated from deposition profiles plotted over an outline of the substrate. The element labels indicate the orientationsof the deposition sources with respect to the substrate. The substrate positions analyzed by XRD are denoted by black points. (b) X-ray diffraction intensities (color scale) as a function of scattering vector (horizontal axis) for measurements taken at various positions (indicated in a), plotted with interpolation as a function of the corresponding x (vertical axis). The observed compositional ranges of peak sets outline the phase fields of the library. The specific compositions of diffraction measurements are noted by small red markers on the composition axis. (c) Representative diffraction patterns from each phase field are plotted to demonstrate phase identification. Reference PDF peaks for labeled phases (Table 1) are plotted in black where relevant. For the $Pt_3Ta + Pt_2Ta$ pattern, PDF 03−1465 is shown in blue and 03−1464 in black. For the Library B $PtTa_4 + Ta$ pattern, the Ta PDF peaks are shown in gray. For the $Pt_2Ta + \beta\ Pt_3Ta$ pattern, the Pt_2Ta (PDF 18−0975) lines are shown in blue with lattice constant reduced by 6% and the β Pt_3Ta lines are shown in black with lattice constant increased by 2%. Relative diffraction intensities are on the same square-root scale across all compositions except that the plot corresponding to fcc-Pt has been multiplied by 0.5.

regions in solutions at a pH of 1. CVs acquired in the absence of fuel provide further characterization of the catalyst, and CVs acquired in the presence of fuel verify the activity of the catalysts in an environment that approaches fuel cell conditions.

To facilitate comparison of oxidation current densities, specific surface area measurements are performed on select catalysts. Because of surface roughness, the active surface area may be much larger than the projected geometric area. As previously described,[22] a linear sweep voltammogram using 1 mM ferrocenemethanol in an aqueous solution of 0.1 M potassium triflate (supporting electrolyte) is used for determining the specific surface area of films. While this technique provides the true electrode surface area available to molecules comparable in size to ferrocenemethanol, the absolute area of Pt surfaces is quantified through analysis of hydrogen adsorption and desorption in 0.1 M H_2SO_4.

Results and Discussion

Structural Characterization. The XRD patterns obtained from the high-throughput crystallography experiments are represented in Figure 1. For Libraries A and B, the set of substrate positions characterized in the XRD experiments are shown as solid black dots on a composition map of the substrate. These diffraction patterns, and the corresponding compositions, are used to generate an interpolated map of diffraction intensity vs $|Q|$ over the composition range of the library. Inspection of these maps reveals several phase boundaries as well as differences in the phase behavior of the two libraries. As seen in Figure 1c, the $Pt_{1-x}Ta_x$ ordered intermetallic phases exhibit a large number of reflections. The typical crystalline grain size of $\lesssim$10 nm results in a relatively broad diffraction peak line widths of $\gtrsim 0.7\ nm^{-1}$. Consequently, many of the reflections overlap both within a given phase and among other phases, which confounds rapid phase identification. The preferred orientation of the crystallites (see fiber texture discussion above) gives rise to additional complexities in interpreting the phase behavior of the libraries. However, analysis of both the correlated shifts in $|Q|$ values of peaks and the appearance or disappearance of peaks as a function of composition assists in phase identification.

The crystallographic phases of the Pt−Ta system are listed in Table 1. In the analysis of Library A, the identification of the fcc-Pt (the pure phase for $x < 0.14$) and $PtTa_4$ (the pure phase for $x > 0.67$) phases is straightforward. From $x = 0.14$ to 0.44, the set of reflections indicates the presence of an orthorhombic phase. As evident in the PDF patterns, orthorhombic Pt_2Ta and Pt_3Ta are distinguished by low-intensity peaks which are observed in all diffraction patterns in this composition range. Although the relative concentrations of the two phases likely change as a function of x, in the present

Table 1. Documented crystallographic phases in the Pt−Ta system and the representative entries from the Powder Diffraction File (PDF).[18] Giessen et al.[23] discuss isomorphism of the two Pt_2Ta phases, and since the orthorhombic phases are not distinguished in our experiments they are given the same abbreviation.

nominal stoichiometry	PDF entry	crystal system	abbreviation in present work
Pt	04−0802	cubic	Pt-fcc
Pt_3Ta	18−0974	monoclinic	β Pt_3Ta
Pt_3Ta	03−1465	orthorhombic	ortho-$Pt_{1-x}Ta_x$
Pt_2Ta	03−1464	orthorhombic	ortho-$Pt_{1-x}Ta_x$
Pt_2Ta	18−0975	orthorhombic	ortho-$Pt_{1-x}Ta_x$
$PtTa_4$	04−1727	tetragonal	$PtTa_4$
Ta	04−0788	cubic	Ta-bcc

Table 2. Results of the XPS Characterization of Library C

				binding energies(eV)		
bulk: x in $Pt_{1-x}Ta_x$	bulk phase	XPS: x in $Pt_{1-x}Ta_x$	XPS: mol frac. TaO_y /(TaO+TaO_y)	Pt $4f_{7/2}$	TaO $4f_{7/2}$	TaO_y $4f_{7/2}$
0.11	Pt-fcc	0.13 ± 0.03	0.26 ± 0.08	71.3 ± 0.3	23.6 ± 0.3	25.9 ± 0.5
0.31	ortho-$Pt_{1-x}Ta_x$	0.42 ± 0.05	0.45 ± 0.12	71.7 ± 0.3	23.6 ± 0.4	26.6 ± 0.4
0.67	NCA	0.89 ± 0.03	0.88 ± 0.08	72.1 ± 0.3	22.6 ± 0.8	25.1 ± 0.5,27.1 ± 0.2

work we simply designate this phase region as ortho-$Pt_{1-x}Ta_x$. This library also contains a phase with little diffraction intensity, other than a broad peak near 27 nm^{-1}. Similar diffraction patterns in this composition range have been presented for films deposited at low temperature.[12,7] Although this unidentified phase may consist of nanometer-scale grains of the high-temperature phase PtTa,[23] the lack of substantial grain growth even at our elevated deposition temperature suggests the possibility that this system forms a metallic glass.[24] Pending further study of this phase we denote it NCA (nanocrystalline alloy). All phases except the NCA phase exhibit strong fiber texture with sharp peaks in the diffraction intensity distribution as a function of angular displacement from substrate normal. For the ortho-$Pt_{1-x}Ta_x$ phases of Library A, our analysis indicates that one or more of the following crystallographic planes are oriented parallel to the film surface: Pt_3Ta (100), Pt_2Ta (010), Pt_2Ta (001).

Library B also contains the $PtTa_4$ intermetallic and an NCA phase but exhibits different phase behavior in the Pt-rich half of the library. For $x < 0.2$, the XRD patterns indicate the presence of an ordered intermetallic phase but the pattern does not match any Pt−Ta entries in the reference literature.[18] Instead of the orthorhombic Pt_3Ta found in Library A, Library B contains monoclinic β Pt_3Ta. The cause for this difference in phase behavior is not understood. The orthorhombic phase is believed to be stabilized by interstitial impurities such as oxygen.[23] Oxygen contamination should increase with the higher background pressure associated with increased deposition temperature, yet the orthorhombic phase is found in the library deposited at lower temperature. A more likely cause is an influence from the underlayer. At the start of the composition spread deposition, the Ta underlayer of Library B may nucleate a different phase than the Ti underlayer of Library A. Once nucleated, the metastable phase can grow indefinitely.

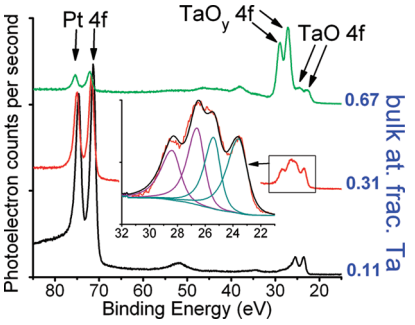

Figure 2. XPS spectra obtained for three $Pt_{1-x}Ta_x$ samples. Each spectrum is labeled on the right with the respective value of x. The inset shows the Ta 4f region of the $x = 0.31$ spectrum with the modeled background and four fitted peaks.

While β Pt_3Ta is present from $x = 0.19$ to above $x = 0.4$, as x increases beyond 0.27 the lattice constant discontinuously increases. At this phase boundary, several new peaks appear, such as the peak labeled p_A in Figure 1c. These peaks are matched by a different orthorhombic structure of Pt_2Ta (03−1464 instead of 18−0975 used for Library A) after a 6% decrease in lattice constant is applied. This pattern also matches well with the peak labeled p_B, but this peak is present for $x < 0.27$ and is the only peak in these β Pt_3Ta diffraction patterns that does not match the monoclinic PDF pattern. The appearance of several new peaks in the diffraction pattern of an ordered intermetallic suggests the addition of a second phase rather than ordering within the existing phase. We thus assert that orthorhombic Pt_2Ta is present on the Ta-rich side of this phase boundary but note that full understanding of phase behavior in Library B will require further analysis.

XPS Characterization. XPS characterizations were performed on Library C. An $x = 0.31$ region of the film was analyzed before electrochemical testing, and following characterization by the fluorescence assay (including pretreatment), the library was diced, and pieces centered at $x = 0.11$, 0.31, and 0.67 were used for analysis. The peak energies and compositions extracted from peak areas are given in Table 2, and we note that for

(23) Giessen, B. C.; Kane, R. H.; Grant, N. J. *Trans. AIME* **1965**, *233*, 855.
(24) Spaepen, F.; Turnbull, D. *Annu. Rev. Phys. Chem.* **1984**, *35*, 241.

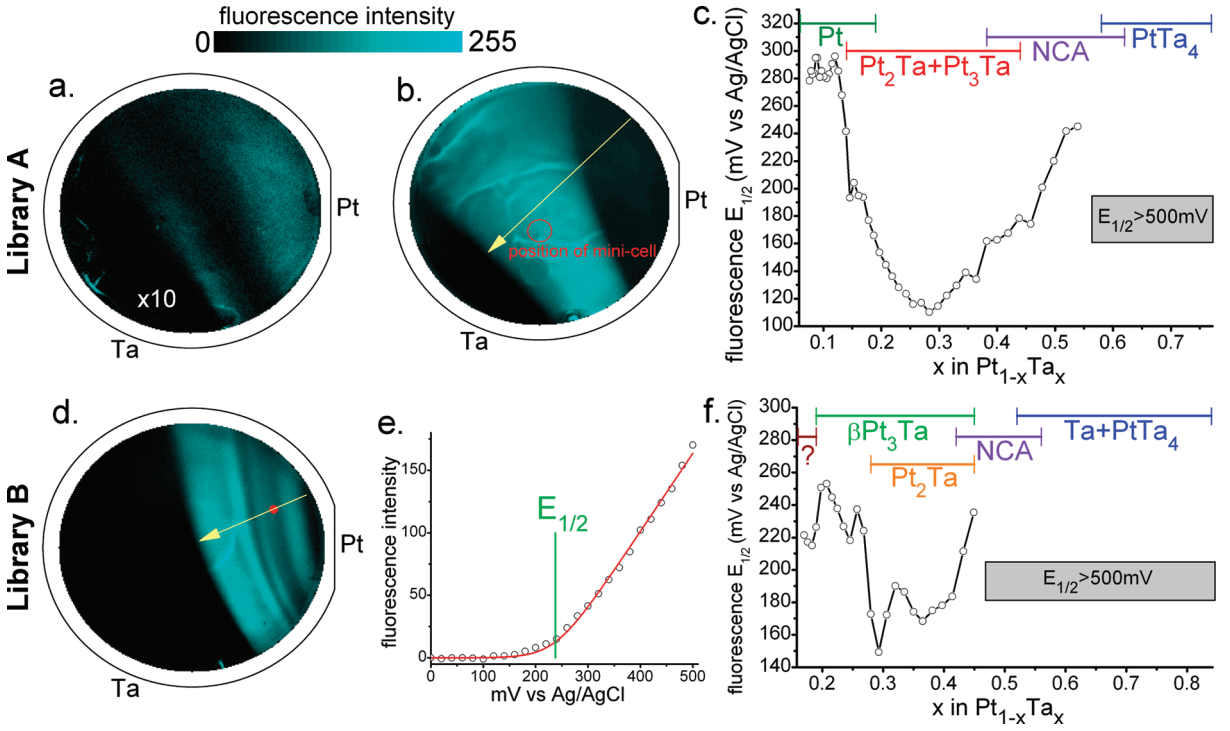

Figure 3. Fluorescence assay measurements of methanol oxidation activity are illustrated for Libraries A (top row) and B (bottom row). (a, b, d) images of the fluorescence intensity across the libraries in an outline of the Si wafer. All three images were acquired at 400 mV during a 5 mV/s anodic sweep. Images b and d were acquired on pretreated libraries and show bright fluorescence from the active regions. Image a was acquired with Library A after days of exposure to air and exhibits much lower fluorescence intensity (the intensity has been increased 10-fold for plotting). The sharp lines of brightest fluorescence (most evident in b) are due to thermally driven convection. (e) Fluorescence intensity profile obtained by averaging the intensity over a 0.5 mm diameter regions (position of white dot in image d), along with the fitted profile (red curve) and fitted value of $E_{1/2}$ (green line). Values of $E_{1/2}$ were also acquired at 1.2 mm spaced points along the yellow lines shown in b and d. (c, f) Plot of $E_{1/2}$ values, along with the composition range occupied by each identified ordered intermetallic phase.

the $x = 0.31$ film, the differences in these quantities before and after electrochemical testing are negligible. The invariance of $x = 0.31$ XPS measurements indicates that any chemical surface modification that occurred during electrochemical testing was reversed upon re-exposure to ambient conditions.

The XPS measurements indicate that the film surface is enhanced in Ta compared to the bulk, which suggests that the chemical potential gradient provided by surface oxidation of Ta is sufficient to cause nanometer-scale diffusion of Ta to the surface. This effect is driven by the high heat of formation of TaO_y compared to PtO_z and was observed in the $Pt_{1-x}Ta_x$ thin films of Bonakdarpour et al.[7]

The binding energy of the Pt $4f_{7/2}$ peak increases with increasing x and exceeds the 70.9 eV value for pure Pt, indicating partial charge transfer from Pt or a lattice strain effect. We note that in the event that the d-electron density decreases via electron transfer to TaO_y, the Pt−CO binding energy would increase.

The Ta 4f binding energies also shift to positive potentials, but we consider the effect of electron transfer with Pt to be negligible compared to Ta−O interactions. Kerrec et al.[25] studied the increase in binding energy with increasing Ta oxidation and associated the Ta $4f_{7/2}$ binding energies 23.5 ± 0.4 eV, 26.1 ± 0.4 eV, and 27.1 ± 0.2 eV with TaO_y stoichiometries $y = 1$, $1 < y \leq 2$, and $y = 2.5$, respectively.

Using these associations, we find that for each Ta concentration, the top few nm of the $Pt_{1-x}Ta_x$ films contain both Ta^{II} and Ta in a higher oxidation state (higher binding energy). The fraction of the Ta in a higher oxidation state is listed in Table 2 and increases as expected with x. The spectra from the $x = 0.11$ and $x = 0.31$ samples were both well fit by one set of high energy peaks while the $x = 0.66$ spectrum required two sets of such peaks to account for the observed data (see Figure 2). Although all three spectra have a peak associated with $1 < y < 2.5$, only the $x = 0.66$ sample has a peak associated with fully oxidized Ta, i.e., $y = 2.5$.

Methanol Oxidation Activity by Fluorescence Assay. Fluorescence assays were performed on the libraries both before and after electrochemical pretreatment. For Libraries A and B, the results are summarized in Figure 3, and we note that the fluorescence intensity contours of Figure 3b,d correspond closely to the composition contours of Figure 1a. The composition ranges associated with the ordered intermetallic phases (identified above) are plotted along with the composition dependence of the catalytic activity in Figure 3c,f. Dramatic correlations between the phase boundaries and the catalytic activity are apparent, and detailed analysis of the figures reveals that the structure−activity correlation is stronger than the composition-activity correlation. The materials with

(25) Kerrec, O.; Devilliers, D.; Groult, H.; Marcus, P. *Mater. Sci. Eng.* **1998**, *B55*, 134.

highest methanol oxidation activity are found in Library A and have the ortho-$Pt_{1-x}Ta_x$ structure with $0.24 < x < 0.32$. A region with $x \approx 0.3$ was chosen for further electrochemical testing as described in the following section. We focus further discussion of the fluorescence assay results on materials from Library A.

Without the reducing pretreatment, the section of the library with only ortho-$Pt_{1-x}Ta_x$ is largely inactive for methanol oxidation. The fcc region as well as the ortho-$Pt_{1-x}Ta_x$ + NCA two-phase region have slightly lower $E_{1/2}$ compared to a typical Pt film. After the pretreatment, the fcc-Pt phase region exhibits a 60 mV decrease in $E_{1/2}$, the NCA region exhibits a 90 mV decrease in $E_{1/2}$, and the ortho-$Pt_{1-x}Ta_x$ region exhibits a decrease in $E_{1/2}$ of more than 300 mV, making it by far the most active catalyst in the library. After exposing the library to air for several days, we repeated the fluorescence assay tests and found that the same activity profile is observed both before and after pretreatment. This experiment was also performed several times on Library B with similar results. We therefore infer that the remarkable improvement in the activity of the ortho-$Pt_{1-x}Ta_x$ catalyst is related to the reduction of the surface from its air-stable state and that the reduction and reoxidation are reversible and reproducible. Although the XPS characterization demonstrates that the top few nm of the $x = 0.31$ air-stable film contain approximately equal concentrations of two Ta suboxides, the electrochemical tests indicate that the most active surface is further reduced. The structure−activity correlation suggests that the reduction of the surface and/or the stabilization of the reduced surface is enabled by the presence of an underlying orthorhombic ordered intermetallic.

Further Electrochemical Study of Optimal Composition. A $Pt_{0.7}Ta_{0.3}$ region of Library A (outlined in Figure 3b) was characterized by local electrochemical tests. In Figure 4, the CVs of a pure Pt sample and the $Pt_{0.7}Ta_{0.3}$ sample are shown for pH 1 solutions containing no fuel, methanol, and formic acid. Comparison of the CVs obtained for each film in the three solutions provides insights into the chemical state and morphology of the $Pt_{0.7}Ta_{0.3}$ surface. The CV of $Pt_{0.7}Ta_{0.3}$ in the 0.1 M H_2SO_4 solution contains the redox waves and hydrogen adsorption/desorption waves similar to those of a pure Pt electrode, in stark contrast to well-studied Pt alloys such as Pt−Ru. As expected, these features are also seen in the Pt film CV, and for both films the hydrogenadsorption and desorption waves are used to calculate electrochemical surface areas of 0.23 ± 0.06 and 1.15 ± 0.1 cm^2 for Pt and $Pt_{0.7}Ta_{0.3}$, respectively. Compared to the film area accessed by the cell (0.32 cm^2), these measurements imply specific surface area ratios (roughness factors) of 0.72 and 3.6. The subunity value of the specific surface area of the Pt film is indicative of surface contamination which likely remained during the subsequent fuel oxidation studies. For the present discussion, we note that the microscopic $Pt_{0.7}Ta_{0.3}$:Pt area ratio determined by hydrogen adsorption is approximately 5:1. The surface area ratio between the same region in the Library A and the same Pt film was also measured via linear sweep voltammetry with a ferrocenemethanol redox couple as described above. This surface area ratio, 1.02 ± 0.16, corresponds to an approximately equivalent surface area accessible by the ferrocenemethanol molecule on the two electrodes. As described in the Supporting Information, this roughness factor is an agreement with the 1.1 value determined by atomic force microscopy (AFM) characterization of the film surface. The ensemble of measurements advocates a model of the surface in which Pt and TaO_y contain $\lesssim$1 nm scale features that are not observed by the ferrocenemethanol redox couple or AFM measurements but give rise to an increased hydrogen adsorption Pt surface area. For calculating the oxidation current densities of small organic molecules, we assume a unit specific surface area ratio.

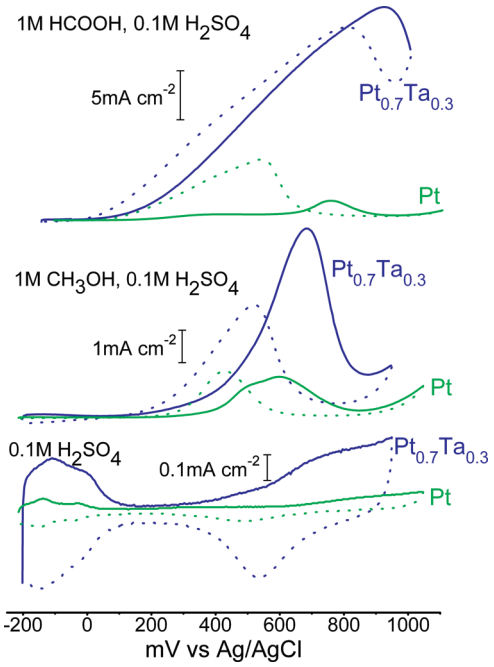

Figure 4. Cyclic voltammograms of Pt and $Pt_{0.7}Ta_{0.3}$ in 1 M formic acid, 0.1 M sulfuric acid; 1 M methanol, 0.1 M sulfuric acid; and 0.1 M sulfuric acid. The forward scans are shown with solid lines and the reverse scans with dotted lines. The CV of $Pt_{0.7}Ta_{0.3}$ in 0.1 M sulfuric acid is indicative of a polycrystalline Pt electrode. The ensemble of characterizations indicate that this electrode contains a high density of Pt islands surrounded by TaO_y.

On the anodic sweep, the methanol oxidation onset potential of the $Pt_{0.7}Ta_{0.3}$ catalyst is $\lesssim$80 mV lower than Pt, a smaller improvement than anticipated from the fluorescence results. The strong effect of the pretreatment step in the fluorescence testing and its assumed influence on nature of the surface oxide raises the question of whether this discrepancy is due to a difference in the pretreated surface oxide in pH 1 vs pH 4 testing solution. Although further investigation of the electrochemical properties of Pt−Ta surfaces may address this issue, the CVs of methanol and formic acid oxidation confirm that the presence of the surface oxide results in higher oxidation current densities. In addition, application of the model of Manoharan and Goodenough[26] to the CVs in

(26) Manoharan, R.; Goodenough, J. *J. Mater. Chem.* **1992**, *2*, 875.

methanol and formic acid indicates that a higher fraction of the fuel is being completely oxidized. That is, in contrast to those of Pt, the CVs on $Pt_{1-x}Ta_x$ demonstrate a greater forward oxidation peak height than reverse peak height. This difference is indicative of a diminished accumulation of carbonaceous species on the surface from incomplete fuel oxidation.

The model of sub-nanometer surface structure proposed to explain the surface area measurements and the strong correlation between fluorescence onset potential and the presence of ortho-$Pt_{1-x}Ta_x$ present the possibility that the partially oxidized surface maintains a structure dictated by the underlying lattice. Future catalyst characterization by surface-sensitive (grazing incidence) XRD and scanning tunneling microscopy characterization will provide insight into this matter, and surface conductivity mapping via the latter technique may provide a better understanding of the Ta suboxide. However, we note that the desired surface condition is one that may be difficult to reproduce outside of the electrochemical environment.

Conclusions

Catalytic activity in the Pt−Ta system was investigated through extensive structural and electrochemical characterization. Thin film libraries containing Pt−Ta ordered intermetallics, a nanocrystalline phase, and an fcc-Pt alloy were tested as methanol oxidation catalysts with a parallel screening method. A reductive pretreatment step, similar to that of typical fuel cell start-up procedures, significantly improved the activity of the catalysts for methanol oxidation. The correlation of activity with the inferred phase fields suggests that the formation of a bulk orthorhombic structure facilitates the partial reduction of the surface TaO_y. The substantial improvement in catalytic activity is attributed to interactions between surface Pt and Ta suboxides, motivating the study of such composite surfaces in the search for superior fuel oxidation catalysts.

The most active catalyst surface appears to be a Ta suboxide and Pt composite with $\lesssim$1 nm structure, and the interaction between these species results in less Pt contamination by carbonaceous species during the oxidation of methanol and formic acid.

Acknowledgment. This work was performed under the Cornell Fuel Cell Institute funded by the Department of Energy (ER06-02-13022-11751-11792). This work made use of the XPS and AFM facilities of the Cornell Center for Materials Research with support from National Science Foundation (NSF) award DMR-0520404. The diffraction experiments were conducted at the Cornell High Energy Synchrotron Source (CHESS), which is supported by NSF award DMR-0225180. The authors thank Jon Shu and Steven Kriske for assistance with the XPS and AFM experiments and Darren Dale and Alexander Kazimirov for assistance with the diffraction experiments.

Supporting Information Available: The composition mapping by XRF and EDS measurements as well as fiber texture analysis, AFM characterization, and photograph of Library A (PDF). This material is available free of charge via the Internet at http://pubs.acs.org.